 CMES, vol.10, no.3, pp.239-247, 2005

Computational Characterization and Evaluation of Deformation Behavior of Spherulite of High Density Polyethylene in Mesoscale Domain

Y. Tomita[1], **M. Uchida**[1]

Abstract: In this study, we clarified the micro- to mesoscopic deformation behavior of a semicrystalline polymer by employing a large-deformation finite element homogenization method. The crystalline plasticity theory with a penalty method for the inextensibility of the chain direction and the nonaffine molecular chain network theory were applied for the representation of the deformation behavior of the crystalline and amorphous phases, respectively, in the composite microstructure of the semicrystalline polymer. The 3D structure of lamellae in the spherulite of high-density polyethylene was modeled, and the tensile and compressive deformation behaviors were investigated. A series of computational simulations clarified the difference in the degree of strain hardening between tension and compression due to different directional chain orientations. In the spherulite, localized deformation occurred depending on the initial distribution of the lamella direction. Due to their interaction with their surrounding, the individual material points of the mesoscopic domain showed a conservative response as compared with that of the unit cell, and a nonuniform response depending on the location of a material point is observed; these are typical mesoscopic responses of semicrystalline polymers.

keyword: Spherulite, HDPE, Multiscale Model, Mesoscale Model, Homogenization Method, Nonaffine Molecular Chain Network Theory, Crystalline Plasticity

1 Introduction

To enable the wide use of semicrystalline polymers as structural materials, the characterization of their mechanical behaviors is indispensable. Semicrystalline polymers have a very complex hierarchical structure, and their microstructure is that of a two-phase composite material consisting of a crystalline lamella and an amorphous layer. In the crystalline phase, molecular chains are oriented in a specific direction. And it has an inextensibility to the chain direction. Spherulite is formed with a radial arrangement of broad thin lamellae, which grow radially accompanied by twist [Lin and Argon (1994)]. Although the deformation mechanisms of the microstructure strongly depend on the directions of the molecular chains and lamella interface, the macroscopic deformation behavior still exhibits initial isotropy [Bowden and Young (1974)].

In accordance with the above characteristics of semicrystalline polymers, simplified models have been proposed to reproduce experimental results [Lee, Parks and Ahzi (1993), Van Dommelen, Parks, Boyce, Brekelmans and Baaijens (2003)]. In these studies, interaction laws based on the Taylor, Sachs and self-consistent models were employed to relate microscopic and macroscopic deformations. The initially isotropic response by modeling the aggregation of randomly oriented composite microstructures is realized. However, these models cannot be used in evaluating the interactions between adjacent composite phases that exhibit a largely scattered local rotation and lamella deformation on the mesoscopic scale, as clarified by AFM observation, depending on the initial orientation and degree of deformation of lamellae due to the applied deformation [Yashiro, Kanai and Tomita (2004)]. Therefore, these characteristic deformation behaviors on the micro- to mesoscopic scales are essential in evaluating the local deformation behavior of semicrystalline polymers.

To this end, based on the experimental evidence, we generated a 2D mesoscopic structure using a Voronoi polygon consisting of composite microstructures with different lamella interface directions [Tomita and Uchida (2005)]. The constitutive equation at each material point of the Voronoi polygon was assigned using the homogenized constitutive equation of unit cell [Higa and Tomita (1999), Okada, Fukui and Kumazawa (2004), Yang and Becker (2004)]. The developed multiscale 2D model was used to evaluate the interactions between the microstructure and the heterogeneous deformation behavior on the

[1] Kobe Univ., 1-1, Rokkodai, Nada Kobe JAPAN.

micro- to mesoscopic scales, and we clarified that the interaction with the surrounding is very important in the evaluation of the mesoscopic deformation behavior of a semicrystalline polymer [Tomita and Uchida (2005)]. However, due to the restriction of the 2D model, the essential 3D feature of the microstructure and its evolutions are still unclear.

In this paper, we generalize our 2D model to a 3D model in order to represent the complex 3D structure of lamellae in the spherulite and to consider all slip systems in the crystalline phase that have a different resistance to slip deformation [Lee, Parks and Ahzi (1993)]. Therefore, we will first provide constitutive equations for individual phases, namely, crystalline and amorphous phases. Then, we will generate the 3D mesoscopic structure consisting of twisted composite microstructures with different lamella interface directions. The constitutive equation at each material point of the microstructures is assigned using the homogenized constitutive equation of a unit cell. Thus, we will evaluate the interaction between such microstructures and the heterogeneous deformation behavior on the micro- to mesoscopic scales of high-density polyethylene (HDPE) under uniform tension and compression.

2 Constitutive Equation

Here, in order to describe the deformation behavior of semicrystalline polymer, the crystalline plasticity theory [Peirce, Asaro and Needleman (1983)] with the penalty method to introduce inextensibility of the chain direction and the nonaffine molecular chain network theory [Tomita, Adachi and Tanaka (1997)] are employed for crystalline and amorphous phases, respectively. Hereafter, the indices "C" and "A" are used for the representation of the quantities for crystalline and amorphous phases, respectively.

The total strain rate d_{ij} is assumed to be decomposed into the elastic strain rate d^e_{ij} and plastic strain rate d^p_{ij}. With Hooke's law for the elastic strain rate d^e_{ij}, the constitutive equation that relates the rate of Kirchhoff stress $\dot{S}_{ij}$ to strain rate d_{ij} becomes

$$d_{ij} = d^e_{ij} + d^p_{ij}, \quad \dot{S}_{ij} = D^e_{ijkl} d^e_{kl} - F_{ijkl} d_{kl},$$
$$F_{ijkl} = \frac{1}{2}\left(\sigma_{ik}\delta_{jl} + \sigma_{il}\delta_{jk} + \sigma_{jl}\delta_{ik} + \sigma_{jk}\delta_{il}\right),$$

where D^e_{ijkl} is the elastic stiffness tensor and σ_{ij} is the Cauchy stress.

The plastic strain rate d^p_{ij} in the crystalline phase is modeled using the crystalline plasticity theory [Peirce, Asaro and Needleman (1983)], with shear strain rate $\dot{\gamma}^{(\alpha)}_{pC}$ on the αth slip system expressed by a power law [Hutchinson (1976)], as

$$d^p_{ij} = \sum_{(\alpha)} P^{(\alpha)}_{ij} \dot{\gamma}^{(\alpha)}_{pC}, \quad \dot{\gamma}^{(\alpha)}_{pC} = \dot{\gamma}_{0C} \frac{\tau^{(\alpha)}}{g^{(\alpha)}} \left| \frac{\tau^{(\alpha)}}{g^{(\alpha)}} \right|^{\frac{1}{m}-1} \tag{1}$$

where $\dot{\gamma}_{0C}$ is the reference strain rate in the crystalline phase, m is the strain rate sensitivity exponent, $g^{(\alpha)}$ is the resistance to slip, $\tau^{(\alpha)} = P^{(\alpha)}_{ij}\sigma_{ij}$ is the resolved shear stress, $P^{(\alpha)}_{ij} = (s^{(\alpha)}_i m^{(\alpha)}_j + m^{(\alpha)}_i s^{(\alpha)}_j)/2$ is the Schmidt tensor, and $s^{(\alpha)}_i$ and $m^{(\alpha)}_i$ are unit vectors along the slip direction and the slip plane normal, respectively. Here, the penalty method is employed to approximately satisfy the inextensibility of the chain direction. The corresponding constitutive equation of the crystalline phase is expressed as [Tomita and Uchida (2002,2005)]

$$\dot{S}_{ij} = \left(D^e_{ijkl} - F_{ijkl} - \lambda_0 c_i c_j c_k c_l\right) d_{kl} - \sum_{(\alpha)} R^{(\alpha)}_{ij} \dot{\gamma}^{(\alpha)}_{pC},$$
$$R^{(\alpha)}_{ij} = D^e_{ijkl} P^{(\alpha)}_{kl} + \left(W^{(\alpha)}_{ik}\sigma_{kj} + \sigma_{ik} W^{(\alpha)}_{kj}\right) \dot{\gamma}^{(\alpha)}_{pC},$$
$$W^{(\alpha)}_{ij} = \frac{1}{2}\left(s^{(\alpha)}_i m^{(\alpha)}_j - m^{(\alpha)}_i s^{(\alpha)}_j\right), \tag{2}$$

where λ_0 is the penalty constant which has a large value, and physically, it represents the chain directional stiffness. c_i is the unit vector of chain direction.

Subsequently, the plastic strain rate d^p_{ij} in the amorphous phase is modeled using a nonaffine eight-chain model [Tomita, Adachi and Tanaka (1997)], with plastic shear strain rate $\dot{\gamma}_{pA}$ [Argon (1973)], as

$$d^p_{ij} = \frac{\dot{\gamma}_{pA}}{\sqrt{2}\tau^*}\hat{\sigma}'_{ij}, \quad \tau^* \equiv \left(\hat{\sigma}'_{ij}\hat{\sigma}'_{ij}\right)^{\frac{1}{2}}, \quad \hat{\sigma}_{ij} = \sigma_{ij} - B_{ij},$$
$$\dot{\gamma}_{pA} = \dot{\gamma}_{0A} \exp\left[\left(-\frac{A\tilde{s}}{T}\right)\left\{1 - \left(\frac{\tau^*}{\tilde{s}}\right)^{\frac{5}{6}}\right\}\right], \tag{3}$$

where $\dot{\gamma}_{0A}$ and A are constants, T is the absolute temperature, τ^* is the applied shear stress, $\tilde{s} = s_0 + \alpha p$, $s_0 = 0.077\mu/(1-\nu)$ is the athermal shear strength [Boyce, Parks and Argon (1988)], p is the pressure, and α is a pressure-dependent coefficient. Furthermore, B_{ij} in Eq. (4) is the back-stress tensor and the principal components

b_i are expressed, by employing the eight-chain model [Arruda and Boyce (1993)], as

$$b_i = \frac{1}{3} C^R \sqrt{N} \frac{V_i^2 - \lambda^2}{\lambda} \mathcal{L}^{-1}\left(\frac{\lambda}{\sqrt{N}}\right), \tag{4}$$

where $\lambda^2 = (V_1^2 + V_2^2 + V_3^2)/3$, V_i is the principal plastic stretch, N is the average number of segments in a single chain, $C^R = nk_BT$ is a constant, n is the number of chains per unit volume, k_B is Boltzmann's constant, and $\mathcal{L}(x) = \coth(x) - 1/x$ is the Langevin function. In the nonaffine eight-chain model [Tomita, Adachi and Tanaka (1997)], the change in the number of entangled points, in other words, the average number of segments N, may change depending on the distortion ξ which represents the local deformation of a polymeric material. The simplest expression of the number of entangled points is $N = N_0 \exp\{c(1-\xi)\}$ with $\xi = 1$ in the reference state, and N_0 is the number of segments in a single chain in the reference state and c is a material constant.

3 Computational Model

As indicated, the spherulite in the semicrystalline polymer is formed with a radial arrangement of broad thin lamellae that grow radially accompanied by twist [Lin and Argon (1994)]. To establish a multiscale model of the spherulite in the semicrystalline polymer, we employ the constitutive equations discussed in the previous chapter and homogenization method for a large-elastoviscoplastic-deformation behavior [Higa and Tomita (1999), Tomita and Wei Lu (2002)]. Figure 1(a) indicates the mesoscopic structure of the spherulite, which is assumed to consist of mesoscopic elements shown in Fig. 1(b) with the spatial repetition of the base cell shown in Fig. 1(c). Assuming that the unit cell is sufficiently smaller than the mesoscopic structure, the coordinates x_i for the mesoscopic structure and the local coordinates y_i for the cell are introduced. The central region of spherulite shown in Fig. 1(a) is modeled using isoparametric finite elements under symmetric boundary conditions with respect to the coordinate achieving mesoscopically homogeneous deformation.

A periodically stacking structure consisting of the crystalline and amorphous phases is given in all Gauss integration points of the mesoscopic finite elements, as schematically illustrated in Fig. 1 (b). This stacking structure can be produced by applying periodic conditions in all y_i directions for the unit cell shown in the lower part of Fig. 1 (c). To construct the part of the spherulite formed with a radial arrangement of broad thin lamellae in which b-axis grows radially accompanied by twist of lamella, we assign the orientation of the y_2 direction parallel to the b-axis in fig. 1 (c) for the unit cell of a mesoscopic element on the basis of the location of the element and relative angle with respect to the center of the spherulite. On the other hand, depending on the relative distance of the element and periodicity of the spiral, we rotate the y_1 and y_3 coordinate directions, and assign the lamella normal of the unit cell. The c-axis in unit cell, schematically illustrated in fig. 1 (c), represents the chain direction, where inextensibility constraint is enforced. The crystalline structure of HDPE exhibits an orthorhombic structure that has four chain slip directions and four transverse slip directions perpendicular to the chain directions. Furthermore, the plane $\{201\}$ is the boundary plane of the amorphous and crystalline phases [Lee, Parks and Ahzi (1993)]; therefore, the direction difference of 30° is assigned in the lamella normal and initial chain directions (c-axis). The direction of a-axis is normal to b- and c-axes. Then a mesoscopically uniaxial tensile and compressive strain rate of $E_0 = 10^{-5}/s$ was applied.

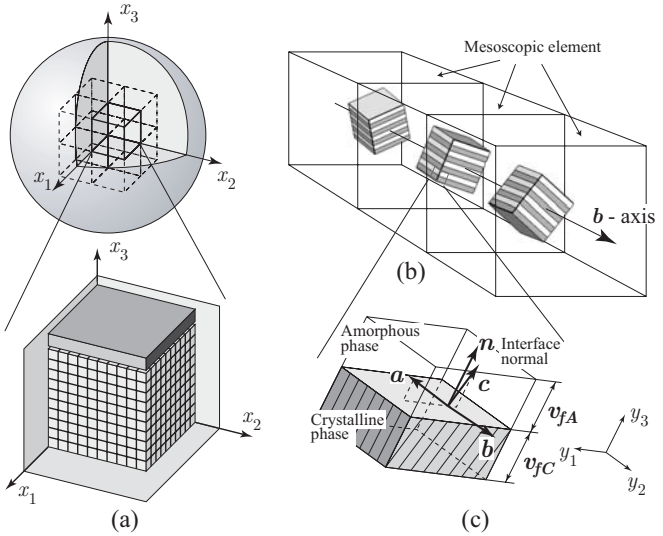

Figure 1 : Computational Model for Homogenization Methods. (a)Mesoscopic structure, (b)Lamella stacking structure, (c)Microscopic structure

The material parameters are specified from references [Lee, Parks and Ahzi (1993), Van Dommelen, Parks, Boyce, Brekelmans and Baaijens (2003), Tomita, Adachi

and Tanaka (1997)]. For the amorphous phase, $E_A/s_0 = 23.7$, $As_0/T = 3.64$, $\alpha = 0.01$, $\dot{\gamma}_{0A} = 1.3 \times 10^{-6}/s$, $s_0 = 4.4$MPa, $C^R/s_0 = 0.36$, $\sqrt{N}$ and $c = 0.1$, and for the crystalline phase, $\dot{\gamma}_{0C} = 1 \times 10^3/s$, $\tau_0 = 8.0$MPa, $1/m = 9$; the components of anisotropic elastic modulus $D^c_{aaaa}/\tau_0 = 0.88 \times 10^3$, $D^c_{cccc}/\tau_0 = 10.13 \times 10^3$, $D^c_{aabb}/\tau_0 = 0.48 \times 10^3$, $D^c_{aacc}/\tau_0 = 0.59 \times 10^3$, $D^c_{abab}/\tau_0 = 0.19 \times 10^3$ and $D^c_{acac}/\tau_0 = 0.20 \times 10^3$ are employed at a temperature $T = 256$K. Here, the subscripts a, b and c for anisotropic elastic modulus correspond to the axes of the HDPE crystalline lattice shown in Fig. 1(c), respectively. The slip system and normalized resistance of HDPE are shown in Table 1 [Lee, Parks and Ahzi (1993)]. Furthermore, to reproduce sufficient inextensibility and to carry out stable calculation, a penalty constant $\lambda_0 = 10^6$ is employed.

Table 1 : Slip system and normalized resistances $g^{(\alpha)}/\tau_0$ of HDPE [Lee, Parks and Ahzi (1993)]

chain slip		
(100)[001]	(010)[001]	{110}[001]
1.0	2.5	2.5
transverse slip		
(100)[010]	(010)[100]	$\{110\}\langle 1\bar{1}0\rangle$
1.66	2.5	2.2

For the representation of stress state and deformation, we introduce equivalent stress and strain rate for a material point in mesoscopic domain as $\dot{\varepsilon}^2_{eq} = 2d_{ij}d_{ij}/3$, $\sigma^2_{eq} = 3\sigma'_{ij}\sigma'_{ij}/2$, for the unit cell without interaction with surroundings as $\dot{E}^2_{eq} = 2\dot{E}_i\dot{E}_i/3$, $\Sigma^2_{eq} = 3\Sigma'_i\Sigma'_i/2$ and for an average value of the mesoscopic domain as $\dot{\overline{E}}^2_{eq} = 2\dot{\overline{E}}_i\dot{\overline{E}}_i/3$, $\overline{\Sigma}^2_{eq} = 3\overline{\Sigma}'_i\overline{\Sigma}'_i/2$. Here, $\dot{E}_i$ and Σ'_i are the homogenized strain rate and deviatoric part of stress Σ_i over a unit cell and $\dot{\overline{E}}_i$ and $\overline{\Sigma}_i$ are the average strain rate and deviatoric part of stress over a mesoscopic domain, respectively. Similarly, $\sigma_m = \sigma_{ii}/3$, $\Sigma_m = (\Sigma_1+\Sigma_2+\Sigma_3)/3$ and $\overline{\Sigma}_m = (\overline{\Sigma}_1+\overline{\Sigma}_2+\overline{\Sigma}_3)/3$ represent the mean stress for a material point, a unit cell and that of the mesoscopic domain, respectively.

4 Results and Discussion

Initially, we will clarify the deformation behavior of the mesoscopic domain. An initial isotropy of the model was

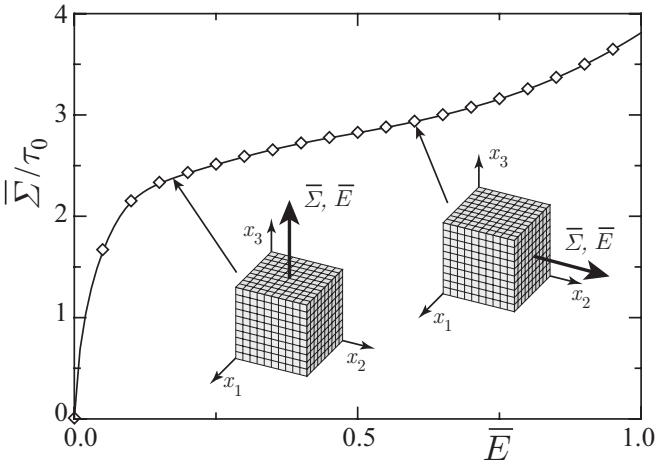

Figure 2 : Isotropy of Mesoscopic Response.

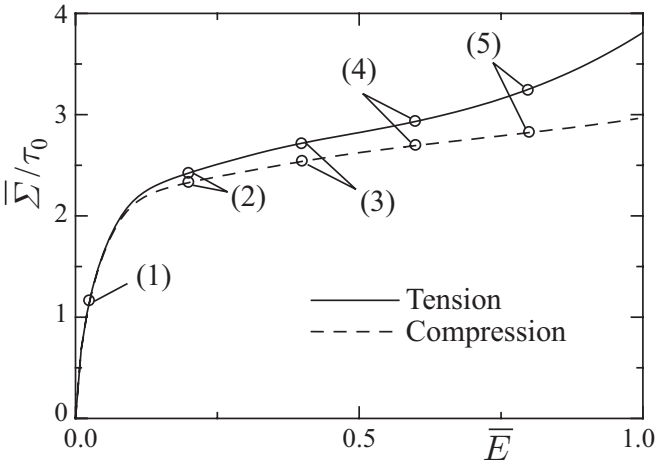

Figure 3 : Mesoscopic True Stress-True Strain Relations.

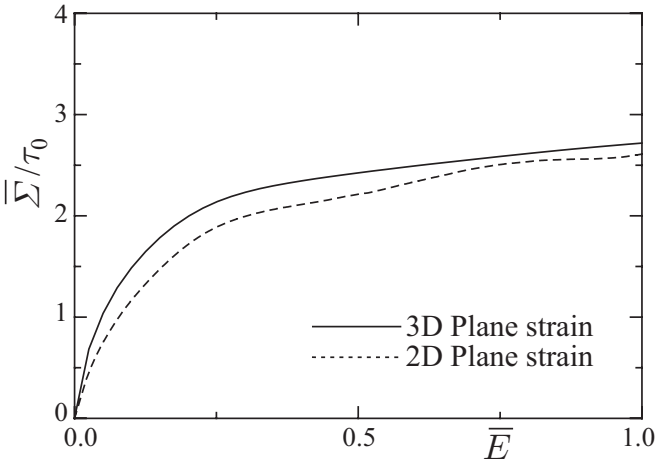

Figure 4 : Comparison Between True Stress-Strain Relations Evaluated by 2D Model [Tomita and Uchida (2005)] and 3D model.

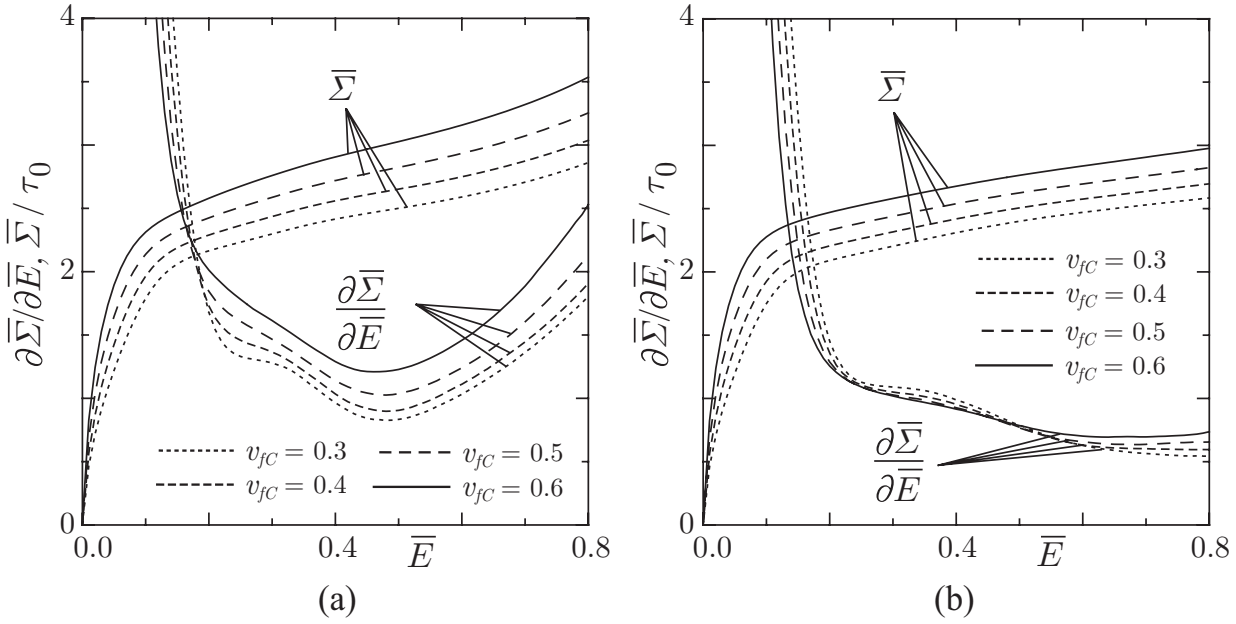

Figure 5 : Effect of Volume Fraction of Crystalline Phase on Stress-Strain Relations. (a) Tension, (b) Compression

examined. Figure 2 shows avarage true stress - true strain relations for x_2- and x_3-directional tension of mesoscopic domain of Fig. 1(a). Regardless of the tension directions, the responses were almost identical; therefore, the isotropic response of the mesoscopic scale in the small to large strain range has been essentially assured.

Figure 3 shows the relationship between the average values of x_3-directional true stress-strain relations for the tension and compression of the mesoscopic domain shown in Fig. 1(a). The nonlinear behavior prior to mesoscopic yielding is attributable to different magnitudes of resolved shear stress in the slip direction, which causes yielding at different stages of deformation. Under tension, strain hardening is shown in the later stage of deformation because of the orientation hardening of the molecular chain in the crystalline and amorphous phases to the stretch direction, which is parallel to the loading direction. However, under compression, the stretch direction is orthogonal to the loading direction. Therefore, orientation hardening does not markedly contribute to the increase in loading directional stress as compared with that in the tension case, which results in moderate hardening even in the later stage of deformation.

Figure 4 shows a comparison of the average values of x_3-directional stress-strain relations evaluated by 2D [Tomita and Uchida (2005)] and 3D simulations with the crystallinity $v_{fC} = 0.5$. To directly compare the 3D and 2D results, the x_1-directional displacement of the material points on the side surface with $x_1 = const.$ was set to be zero and shear free conditions were also enforced on the same surface of the 3D case shown in Fig. 1(a). The mesoscopic structure of the 2D semicrystalline polymer was modeled using a Voronoi polygon consisting of composite microstructures with different lamella interface directions [Tomita and Uchida (2005)], whereas, that of the 3D semicrystalline polymer was modeled using a microstructure with continuously grown lamella distribution in the spherulite. Therefore, the disorderliness of the microstructure of the 3D model is partially restricted, and the resistance to deformation on the mesoscopic scale of the 3D model is higher than that of the 2D model.

Figure 5 indicates the effect of the volume fraction of the crystalline phase on the average value of x_3-directional stress-strain relations, and the hardening rates of the mesoscopic domain under (a) tension and (b) compression. The effect of crystallinity on the stress-strain relations in high-strain regions is predominant in the tension case. Hardening rates are very sensitive to the volume fraction of the crystalline phase under tension, which are intensified by enhancing crystallization. While orientation hardening in a high-strain region under tension is reinforced by enhancing crystallization, the stress-strain relations under compression are almost parallel, because orientation hardening in the crystalline phase does not

markedly contribute to the increase in loading directional stress as mentioned above. This stress-strain behavior is the homogenized behavior of individual material points exhibiting quite different responses depending on the direction of the lamella interface and the interaction of the material points with their surrounding.

To clarify the deformation behavior of the semicrystalline polymer in detail, we evaluate local deformation. Figure 6 indicates the equivalent strain rate $\dot{\varepsilon}_{eq}$ distributions at (1)-(5) in the stress-strain relations shown in Fig. 3(a). The magnitude of the strain rate is normalized by the average value of the mesoscopic domain $\dot{E}_0$. As can be seen in the Fig. 6(1), localized deformation, which depends on the initial lamella structure, occurs prior to mesoscopic yielding. Due to orientation hardening in the amorphous and crystalline phases, and the rotation of the lamella interface direction, the nonuniform deformation accompanied by the onset and propagation of localized deformations in a specific region in the spherulite is observed. These are essential results observed in all cases and attributable to the interaction between the surrounding and the direction of the lamella interface.

Figure 7 indicates the pole figures of the chain directions under (a) tension and (b) compression at stages (1) and (5) indicated in Fig. 3(a). All points are shown in figures (A). Randomly distributed points in the pole figure of the chain direction at stage (1) move toward the principal stretch direction with the deformation and form locally clustering regions. The principal slip system is either the chain slip system or transverse slip system, which depends on the Schmidt factor and resistance to slip on each slip plane. To clarify the effects of the chain slip and transverse slip on the deformation behavior, we separate all the points in the pole figures (A) into (B); left- and right-hand sides in (B) indicate the cases where the principal slip system in the crystalline phase is one of the chain slip systems and one of transverse slip systems, respectively. The slip directions of the chain slip are identical, while those of the transverse slip are different; therefore, as depicted in (B) at stage (1), the points at which the chain slip system is the principal slip system highly concentrate near the loading direction, while the points at which the transverse slip is the principal slip system scatter in the entire region. With the progress of deformation to stage (5), the chain directions, in which the chain slip system drives the plastic deformation of the crystalline phase, particularly rotate toward the stretch direction. Therefore, the chain directions of the principal slip system mainly distribute near the loading direction in stage (1) easily orient to the loading direction, which results in early orientation hardening. On the other hand, orientation hardening is markedly delayed in the compression case, where the loading direction is perpendicular to the principal stretch direction.

When the chain direction completely orients to the stretch direction, the degree of the stiffness in crystalline phase markedly increases due to the inextensibility of the chain direction. Therefore, the deformation of lamellae with a hardened crystalline phase is mainly absorbed in the amorphous phase. As a result, the chain direction in the crystalline phase is slightly misaligned with respect to the principal direction.

Figure 8 indicates the equivalent stress σ_{eq} - strain ε_{eq} relations for the material points in mesoscopic domain, equivalent stress Σ_{eq} - strain E_{eq} relations for unit cells without interaction with surroundings, and average equivalent stress $\overline{\Sigma}_{eq}$ - strain $\overline{E}_{eq}$ relations for the mesoscopic domain. To avoid the complexity of the figure, the stress-strain relations for material points selected in the gray region shown in the inset were displayed. We confirmed that the stress-strain relations for material points generally fall within the range of the scatter of those shown in the figure. This trend is the same as that of mean stress-strain relations. The stress-strain relations of individual material points exhibit very different responses. Several material points with specific lamella interface directions show very significant hardening. An interesting observation is the existence of material points with very large strains and stresses, which are three times well over the average values for the mesoscopic domain. Due to their interaction with their surrounding, individual material points in the mesoscopic domain show a repressed response as compared with the unit cell model, which is typical of the mesoscopic scale. The extremely unique deformation behavior exhibiting softening and hardening observed in the 2D model [Tomita and Uchida (2005)] disappears in the material points of the mesoscopic domain, which is attributable to the relaxation of the constraint of lamella rotation in the 3D model as compared with the 2D model.

Here, we will discuss the mean stress, which is the key parameter for evaluating the possibility of the onset of the formation of defects such as cavitations and crazings. Figure 9 indicates the average mean stress in amorphous

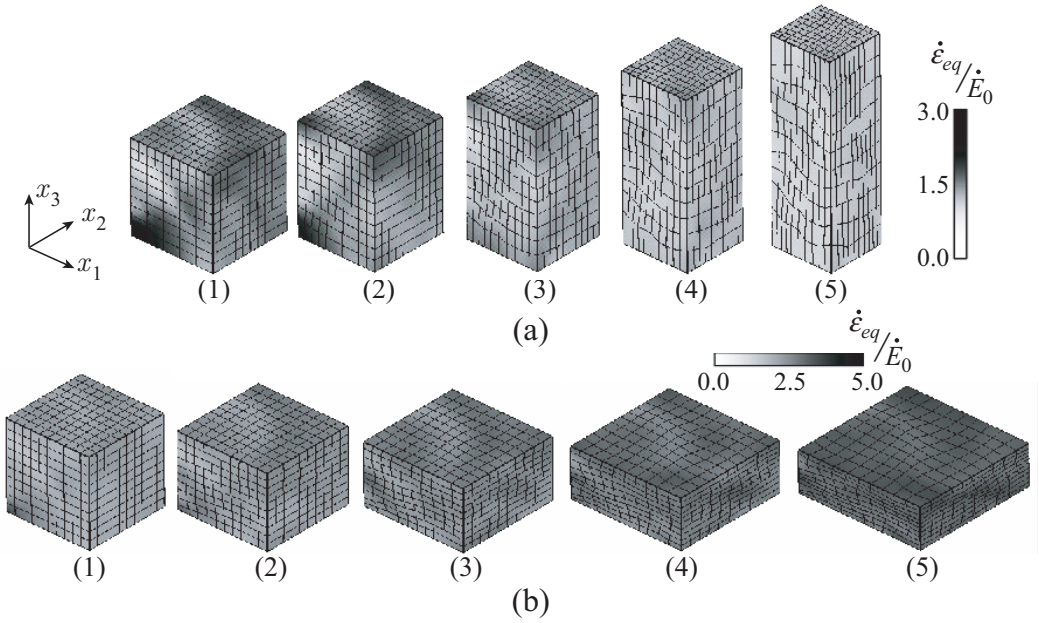

Figure 6 : Equivalent Strain Rate Distributions. (a) Tension, (b) Compression

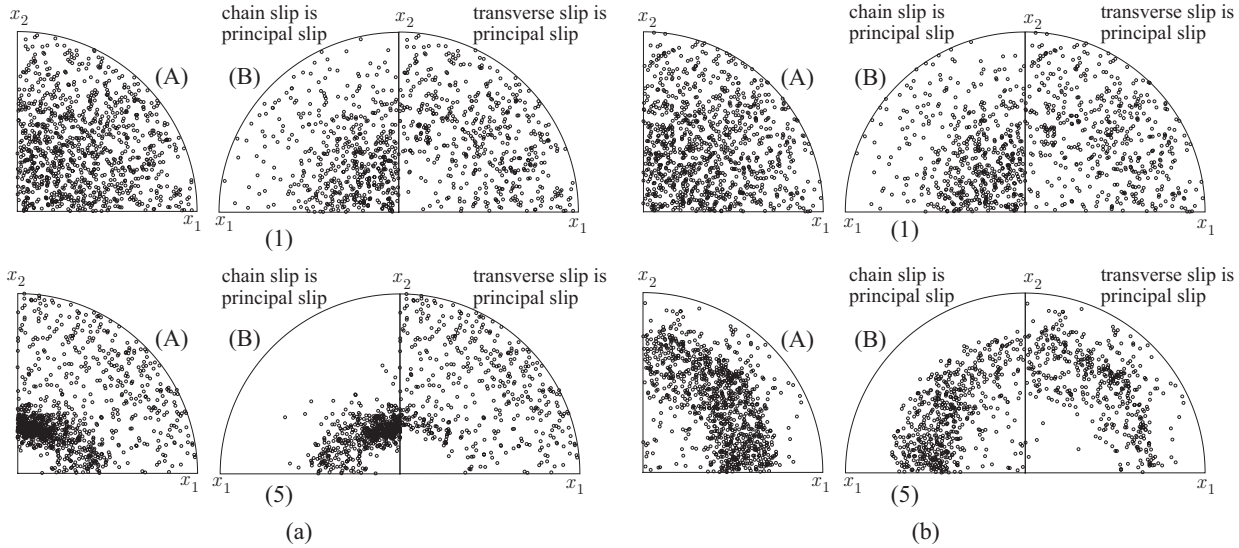

Figure 7 : Pole Figures of Chain Direction. (a) Tension, (b) Compression

phase σ_{mA} - equivalent strain ε_{eq} relations for individual material points of the mesoscopic domain and mean stress in amorphous phase Σ_{mA} - equivalent strain E_{eq} relations for the unit cell. A very scattered distribution including negative mean stresses depending on the location of material points can be seen. The mean stress in the mesoscopic domain is suppressed as compared with the unit cell case, which shows a tendency similar to that observed in the stress-strain relations in Fig. 8. The dispersion of mean stress in the amorphous phase and equivalent strain relations for individual material points in the 3D case is smaller than that in the 2D case [Tomita and Uchida (2005)], which may be attributable to the easiness of the rotation of lamellae in the 3D case, whereas it is limited in a plane in the 2D case. From these results, the local deformations behaviors in the spherulite strongly depend on the initial lamella direction, the constraint of lamella rotation and interaction of material points with their surrounding. Therefore, these suggest the importance of the 3D mesoscopic model in evaluating the local stress and strain that are indispensable for predicting the strength of semicrystalline polymers.

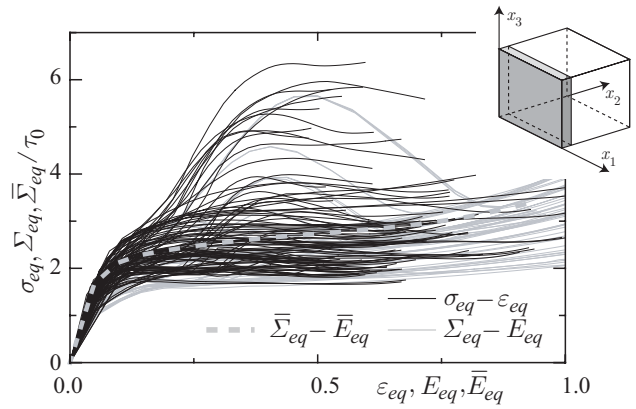

Figure 8 : Equivalent Stress-Strain Relations for Material Points, Unit Cells and Mesoscopic Domain.

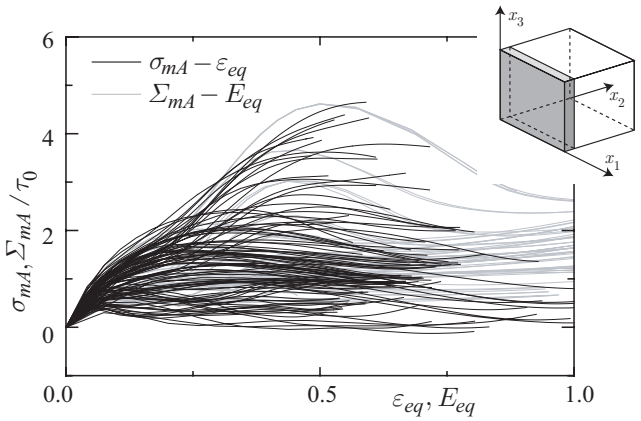

Figure 9 : Mean Stress in Amorphous Phase-Equivalent Strain Relations for Material Points and Unit Cells.

The AFM observation of the rotation of lamellae in the mesoscopic scale of HDPE under tension indicates that the material points essentially rotate in accordance with the rotation of the mesoscopic scale with a very large fluctuation as indicated in Figure 10 [Yashiro, Kanai and Tomita, (2004)]. The present computational simulation is not necessarily the model of the HDPE employed in the experimental study, however, similar tendencies of the local deformation behavior of the lamellae with different directions were observed, which may suggest the validity of the present results.

5 Conclusion

A new 3D multiscale model relating the micro- to mesoscopic deformation behaviors of semicrystalline polymers has been developed by employing a homogenization method, and the characteristic deformation behavior

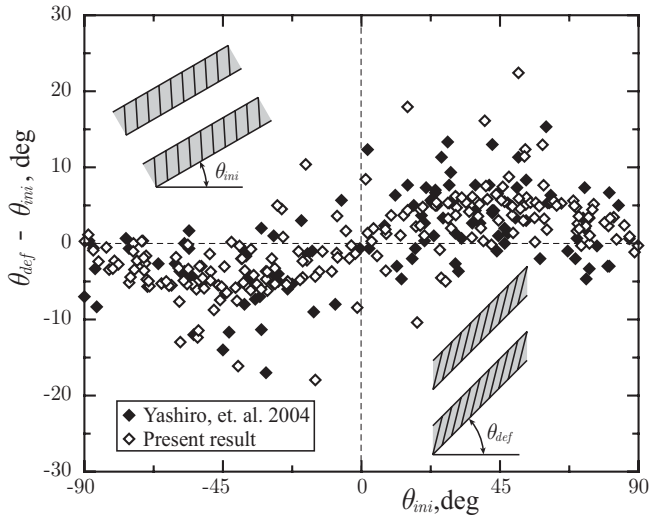

Figure 10 : Rotation of Lamellae in the Mesoscopic Domain. θ_{ini}, θ_{def} are the directions of lamella in initial and deformed states, respectively.

has been clarified. The main results obtained are as follows.

1. The average responses of the present mesoscopic-scale model of semicrystalline polymers are almost identical, regardless of the tension direction, in small to large deformation ranges that ensure the isotropy and validity of the present model.

2. The volume fraction of the crystalline phase significantly affects the average elasticity modulus and yielding stress; however, subsequent hardening under compression is markedly suppressed where the chain direction rotates toward the normal direction to compression.

3. The interaction with the surrounding and orientation hardening of individual material points result in the onset and propagation of mesoscopic nonuniform deformation in the mesoscopic domain.

4. The disorderliness of the microstructure of the 3D model is partially restricted; therefore, the resistance to deformation on the mesoscopic scale of the 3D model is higher than that of 2D model. The fractuation in the local responses in mesoscopic domain is restrained due to the easiness of lamella rotation in 3D model.

5. Equivalent stresses of individual material points in the mesoscopic domain are more conserved than those of unit cells, which is closely associated with the interaction of the material points with their surrounding. Due to the easiness of lamella rotation in 3D model, the anomalous response observed in the unit cells of the 2D model is not seen in the 3D model. The magnitude of mean stress exhibits large scattering as compared with that of equivalent stress.

6. The above-mentioned characteristic features of the deformation behaviors of semicrystalline polymers in the mesoscopic domain and material points, particularly the difference between the two scales, are significant, which should be considered in the evaluation of the strength of semicrystalline polymers.

Acknowledgement: Financial support from the Ministry of Education, Culture, Sports, Science and Technology of Japan through Grant-in-Aid for Scientific Research and Grant-in-Aid for JSPS Research Fellow is gratefully acknowledged.

References

Argon, A. S. (1973): A Theory for the Low-Temperature Plastic Deformation of Glassy Polymers. *Philos. Mag.*, vol.28, pp.839–865.

Arruda, E. M.; Boyce, M. C. (1993): A Three-Dimensional Constitutive Model for the Large Stretch Behavior of Rubber Elastic Materials. *J. Mech. Phys. Solids*, vol.41, pp.389–412.

Bowden, P. B.; Young, R. J. (1974): Deformation Mechanisms in Crystalline Polymers. *J. Mater. Sci.*, vol.9, pp.2034–2051.

Boyce, M. C.; Parks, D. M.; Argon, A. S. (1988): Large Inelastic Deformation of Glassy Polymers, Part I: Rate Dependent Constitutive Model. *Mech. Mater.*, vol.7, pp.15–33.

Higa, Y.; Tomita, Y. (1999): Computational Prediction of Mechanical Properties of Nickel-Based Superalloy with Gamma Prime Phase Precipitates. *Advance Materials and Modeling of Mechanical Behavior*, vol.III, pp.1061–1066, Fleming Printing Ltd.

Hutchinson, J. W. (1976): Bounds and Self-Consistent Estimates for Creep of Polycrystalline Materials. *Proc. R. Soc. Lond. A*, vol.348, pp.101–127.

Lee, B. J.; Parks, D. M.; Ahzi, S. (1993): Micromechanical Modeling of Large Plastic Deformation and Texture Evolution in Semi-Crystalline Polymers. *J. Mech. Phys. Solids*, vol.41, pp.1651–1687.

Lin, L.; Argon, A. S. (1994): Review : Structure and Plastic Deformation of Polyethylene. *J. Mater. Sci*, vol. 29, pp. 294–323.

Okada, H.; Fukui, Y.; Kumazawa, N. (2004): Homogenization Analysis for Particulate Composite Materials using the Boundary Element Method. *CMES: Computer Modeling in Engineering & Sciences*, vol.5, pp.135-150.

Peirce, D.; Asaro, R. J.; Needleman, A. (1983): Material Rate Dependence and Localized Deformation in Crystalline Solids. *Acta Metall.*, vol.31, pp.1951–1976.

Tomita, Y.; Adachi, T.; Tanaka, S. (1997): Modeling and Application of Constitutive Equation for Glassy Polymer Based of Nonaffine Network Theory. *Eur. J. Mech. A/Solids*, vol.348, pp.101-127.

Tomita, Y; Lu, Wei (2002): Characterization of Micro- to Macroscopic Response of Polymers Containing Second-Phase Particles Under Macroscopically Uniform Deformation. *Int. J. Solids Struct.*, vol.39, pp.3409–3428.

Tomita, Y.; Uchida, M. (2005): Computational characterization of micro- to mesoscopic deformation behavior of semicrystalline polymers. *Int. J. Mech. Sci.*, vol.47, pp.687–700.

Uchida, M.; Tomita, Y. (2002): Deformation of Crystalline Polymers Containing Amorphous Phase. *Proc. CMD2002*, pp.111–112, in Japanese.

Van Dommelen, J. A. W.; Parks, D. M.; Boyce, M. C.; Brekelmans, W. A. M.; Baaijens, F. P. T. (2003): Micromechanical Modeling of the Elasto-Viscoplastic Behavior of Semi-Crystalline Polymers. *J. Mech. Phys. Solids*, vol.51, pp.519–541.

Yang, Q. S. ; Becker, W. (2004): A Comparative Investigation of Different Homogenization Method for Prediction of the Mesoscopic Properties of Composites, *CMES: Computer Modeling in Engineering & Sciences*, vol.6, pp.319-332.

Yashiro, K.; Kanai, M.; Tomita, Y. (2004): AFM Study on Deformation Behavior of Polyethylene Lamella Structure by Means of In-situ Bending Test. *J. Soc. Mat. Sci., Japan*, vol.53, pp.1359-1364, in Japanese.